M. P. Manahan Sr and R. B. Stonesifer†*

Miniature Charpy Design Optimization for Reactor Pressure Vessel Surveillance Applications

REFERENCE Manahan, M. P. Sr and Stonesifer, R. B., **Miniature Charpy design optimization for reactor pressure vessel surveillance applications,** *Evaluating Material Properties by Dynamic Testing*, ESIS 20 (Edited by E. van Walle) 1996, Mechanical Engineering Publications, London, pp. 125–147

ABSTRACT As nuclear power plants approach end-of-licence (EOL), there is an ever increasing need to expand the amount of data from the original surveillance specimens. Miniaturized notched specimens are one viable solution to this problem of limited surveillance material. Experiments performed over the past decade have demonstrated that miniature Charpy specimens can be designed to yield transitional fracture behaviour and that the fracture appearance and energy-temperature curves can be quantitatively related to the conventional Charpy specimen data. This paper presents the results of a study focused on designing an optimized miniature specimen and test machine. A combination of literature review, metallurgical analysis, and finite element analysis was used to consider such design parameters as minimum specimen cross-section, specimen length, notch acuity, the use of side grooves, side groove geometry, support span, and striker geometry. Two dimensional and three dimensional, elastic-plastic, large deformation, finite element analyses were used to compare stress/strain fields for standard and miniaturized specimens. Specimen and test machine geometries have been developed to ensure continuum requirements are met, the specimen stress fields simulate those of the conventional specimen, and scatter for the miniature data is minimized.

Introduction

In the past, qualitative (**1**)(**2**)(**3**) interpretations of miniature Charpy data have been proposed to explain differences between the miniature specimen data and the ASTM E23 standard specimen results. The first successful quantitative interpretation of miniature Charpy data was reported in 1990 (**4**). The recently released ASTM STP 1204 (**5**) contains several papers focused on quantification of the miniature Charpy test approaches and data interpretations. With regard to specimen design, Table 1 organizes the miniature Charpy test geometries which have been reported in the open literature into four geometry categories. While there are some minor dimensional variations, the four geometries listed reasonably represent those reported by various researchers. Geometry 1 in Table 1, which was originally developed by the author, has been modified to increase the specimen length to ~25 mm. Further discussion on this specimen design and on side-grooving, follows. Geometries 3 and 4 involve cross-

* MPM Research & Consulting, PO Box 840, Pike Street 915, USA. PA 16851 Lemont, USA.
† Computational Mechanics Inc., 1430 Steele Hollow Road, Julian, PA 16844, USA.

Table 1 Partial list of miniature Charpy specimen geometries

Geometry	*B thickness (mm)*	*W width (mm)*	*L length (mm)*	*Number from one full size*	*Side Grooves*
1	5	5	12.7	16	yes
2	5	5	25.4–27.0	8	no
3	3.3	3.3	25.4	18	no
4	3	4	26.0	12	no

sectional dimensions ~3 mm. However, specimens with 3–4 mm cross-sectional lengths may not yield continuum results for some steels. The effect of microstructure on specimen design is considered later in the paper.

In support of miniature Charpy standardization work, a focused design study has been performed to optimize the miniaturized notched test (MNT) (**4**) for nuclear reactor pressure vessel (RPV) applications. The MNT is a dynamic three point bend test which has been designed to yield data which are quantitatively the same as those obtained in conventional Charpy testing. The key elements of this study are presented here. It is intended that the international standardization effort will lead to accepted standard practices related to miniature specimen geometry, test machine parameters, and data analysis. It is important to emphasize that the specimen size recommendations reported here are only applicable to the US RPV materials. Application to other classes of material must begin with an in-depth understanding of the material microstructure. The appropriate size and specimen geometry can then be determined using a similar approach.

MNT experimental design

Material microstructure impact on specimen design

It is possible to perform an in-depth microstructural study for each material for which a miniaturized Charpy test is to be conducted, and then specimen dimensions can be established on a case-by-case basis. However, a more effective approach would be to define a specimen size which is adequate for determining MNT properties for a defined class of materials. This latter approach has been pursued and will form the basis for specimen size recommendations to the standards committees.

To adequately sample a representative volume of an RPV steel when using MNT specimens, one must know the scale, or mean separation, of the inhomogeneities that exist in the steel plate from which the pressure vessel is fabricated. The term inhomogeneity as used here refers to such compositional and microstructural characteristics as: solute segregation during solidification which leads to bands of variation in mean chemical composition and stringers of inclusions; grain boundaries (grain size); colonies of transformation products; precipitates; and the presence of Fe and alloy carbides. The scale of the inhomogeneities depends upon both compositional and processing variables.

Table 2 Size scale of various microstructural features in reactor pressure vessel steels

Inhomogeneity type	*Scale (mm)*
Chemical banding	0.5–1
Inclusion stringers	~0.5
Austenite grain size (TE)	0.06–0.2
Ferrite grain/pearlite colony size	0.01–0.08
Bainite/martensite colony size	~0.05
Carbide spacing in	
pearlite	0.0001–0.005
bainite	~0.002
martensite	≤0.0001

Base, weld, and heat-affected zone (HAZ) materials were analysed for the US vessel steels to determine the cross sectional dimensions which will ensure adequate material sampling. This analysis was performed to provide a conservative estimate of the minimum MNT specimen cross sectional dimensions so that microstructural measurements are not required for each heat of nuclear reactor pressure vessel material tested.

Base Plate

The size scale of various microstructural features considered for US RPV steels are shown in Table 2. It is concluded that the coarsest inhomogeneity in the base plate is chemical banding that occurs especially in high-Mn steels. The variation in Mn content across the banding leads to the formation of a range of transformation products, and thus a range of properties throughout the plate cross-section. Therefore, the band separation will be the factor which controls minimum specimen size in RPV plates. An approximate relation for the spacing of bands (L) based on the casting size and the total reduction from ingot to plate is: $L = 0.116\ \theta_f$(mm), where θ_f is the plate thickness (expressed in inches) (**6**). Accordingly, high-Mn RPV plates which are typically 4 to 10 inches thick are predicted to contain chemical bands with an average separation of 0.5 to 1.1 mm. Observations on a section of forged A508 plate confirm these predictions (**7**). Stringers of inclusions, which are concentrated in the chemical bands, are the next coarsest inhomogeneity in RPV plate. The primary effect of inclusions (sulfides, oxides, oxy-sulfides) is a loss of ductility (manifested as a decrease in the upper shelf energy (USE)) because of the weakness of the interface between metal and inclusion, and because of the brittleness of the inclusions. The separation of inclusion stringers is somewhat finer than that of the bands since the stringers can form at any point within the rather diffuse band width. Thus, tensile and Charpy specimens designed to sample a volume that will include chemical banding will of necessity include an adequate sample of inclusion stringers.

Other chemical and microstructural inhomogeneities in the plate are on a finer scale than either the bands or stringers and thus will be adequately

sampled by specimens designed to include the coarser inhomogeneities. Accordingly, the cross-sectional dimension of mini-specimens cut from base plate, assuming that five times the coarsest inhomogeneity will provide an adequate sampling, will be dictated by the banding separation which varies with plate thickness. From the above analysis, specimen cross sections will range from 2.5 mm for 4-inch plate to 5 mm for 10-inch plate.

HAZ

Throughout most of the HAZ, there is no massive redistribution of solute during the very short dwell time at high temperature experienced during the weld thermal cycle. Austenite grain size in the coarse grain HAZ (CGHAZ) may approach 0.5 mm in plates of all thicknesses depending on heat input and peak temperature. Thus the scale of temper embrittlement (TE) may be on the same order as the banding (~0.5 mm), and would therefore require specimens taken from the CGHAZ to have a cross-section dimension of at least 2.5 mm. Therefore, the spacing of chemical banding present in the base plate (0.5–1 mm) still remains the controlling factor in determining the cross-sectional dimension of mini-specimens cut from the HAZ.

Weld bead

The grain structure of the weld bead is columnar, the width of the columns being 0.2–0.5 mm. In addition, centreline segregation of impurities often occurs. Specimens should therefore be notched at the centreline to have a cross-section dimension on the order of 2.5 mm or greater.

Based on microstructural considerations, miniature Charpy specimens cut from RPV materials should have minimum cross-sectional dimensions of 5 mm × 5 mm, unless a smaller size can be justified by thorough microstructural characterization. This determination is based on the empirical observation that ~5 times the largest microstructural inhomogeneity is required to ensure continuum response (**4**). Thus, the proposed miniature specimen cross-sectional dimension if 1/2 that of the conventional specimen.

Miniature specimen length

Using the scale factor of 1/2 that was selected for designing the miniature specimen cross-section to select the specimen length would allow 8 miniature specimens (each 27.5 mm long) to be fabricated from the material of one standard Charpy specimen. The experimental work described in (**4**) used specimens with half of this scaled length and therefore allowed 16 miniature specimens (each 13.75 mm long) to be obtained from the material of one standard specimen. Although the experimental data showed good characterization of the transitional fracture behaviour, it is not clear that the stress field of the 13.75 mm long miniature specimen adequately simulates that of the conventional specimen. Therefore, a bending-to-shear stress ratio analysis was performed to determine the optimal specimen length.

The bending-to-shear ratio is just the ratio of the nominal peak bending stress to the shear stress that results from a simple strength of materials analysis of a smooth bar with the same overall dimensions as the fracture specimen. For simply supported rectangular bars, the bending-to-shear stress ratio is 3S/D, where S is the distance between supports, and D is the specimen depth. For the standard Charpy specimen, the ratio is 12. For the 1/16 volume miniature specimens (**4**), the ratio is 7.1. Proportional scaling of cross-sectional dimensions and length by a factor of 1/2 results in the scaled specimen having the same ratio as the standard Charpy specimen.

If the bending-to-shear ratio is sufficiently large, then the form and intensity of the notch and subsequent crack tip fields are effectively determined by the applied bending moment. For smaller specimen span-to-depth ratios, the load required to achieve a given bending moment is increased. For a four point loaded specimen, these larger loads would tend to be of little consequence since the notch region would be under pure bending and the stress and strain concentrations around the load points would be remote to the fracture plane. For the three point bending configuration of the Charpy specimen, however, the striker contact region stress field and associated plastic zone can begin to interact with that of the notch (or crack) if the load levels are sufficiently large. Decreasing the specimen span-to-depth ratio would result in such interaction effects occurring at the lower applied moment. Even with the same span-to-depth ratio, a smaller specimen will require a larger applied load (relative to the yield load for example) than a full scale specimen to achieve the same applied J level. Therefore, even with the same span-to-depth ratio, the interaction between the notch/crack tip fields and the tup contact related fields will occur at a lower level of crack field intensity for the smaller specimen. Using a smaller span-to-depth ratio in a smaller specimen would just compound this undesirable behaviour.

The tendency for the miniature specimens that were used in previous studies (**4**) to fail outside the intended fracture plane when side grooves were not used could have been increased by using a smaller bending-to-shear ratio. The failure of these specimens apparently involved plastic slip along the plastic zone that resulted from the notch region plastic zone linking up with the plastic zone formed in the tup contact region. The contact stresses for a given moment and notch/crack field intensity would have been larger due to the decreased span-to-depth ratio. This would result in correspondingly more intense contact region plastic zones. Another contributing factor to this undesirable failure mode would be the increased level of average shear stress acting in the region where the plastic zones link (average shear stress on the section is proportional to the applied load). This shear stress would tend to promote the type of slip that resulted in the observed failure mode.

As the above discussion shows, the only benefit from using a shorter specimen is the ability to get more miniature specimens from a given amount of material. Since it seems likely that weld reconstruction (**8**) will allow the

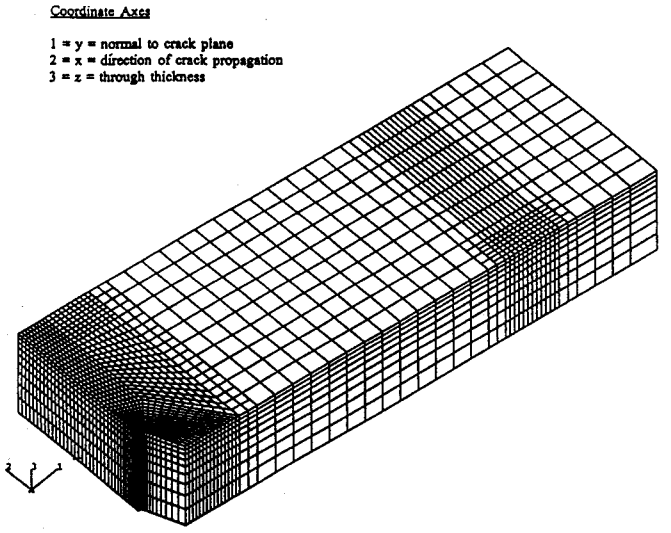

Fig 1 Refined 3D finite element grid of the standard Charpy specimen

benefits of a smaller length (i.e., more specimens), while still allowing the benefits of a proportionately scaled standard specimen, a scale factor of 1/2 was recommended for designing the miniature specimen length.

Stress field characterization

The section describes the results of finite element analyses which were performed to characterize the notch tip stress field.

The plane strain nature of 3D notch region stresses

To determine the degree to which the 3D notch region stresses are plane strain in nature, the stress distributions in the fracture plane were compared to the 2D plane strain solution. The ABAQUS general purpose non-linear finite element code was used to perform these calculations. A typical finite element mesh and coordinate system are shown in Fig. 1. Eight-noded brick elements were used in the analysis and finite strain theory was included in all calculations. The material flow curve was idealized as piece-wise linear. In the discussion which follows, general yield load is defined as the load at which yielding has spread across the entire uncracked ligament. This load corresponds to the 'knee' in the load-deflection curve. In the cases where side-grooves were analysed, a 45 degree included angle was modelled with 20 percent depth.

Figures 2 through 4 show the notch region stress field comparisons for the three applied displacement levels of 0.2 (near general yield), 1.5, and 3.0 mm (near peak load). In order to determine the dependence of the behaviour on

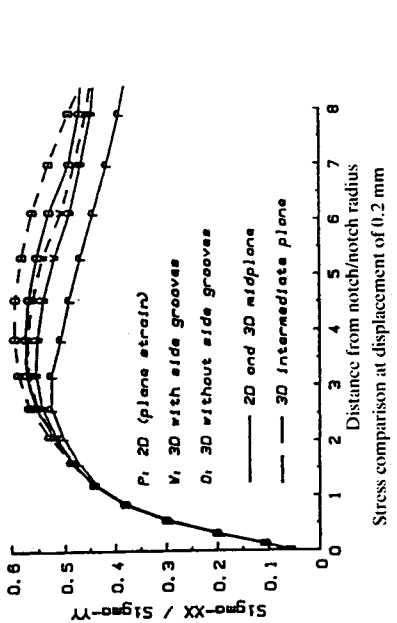

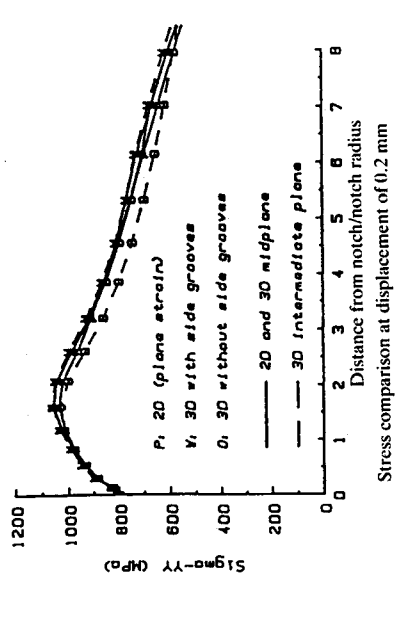

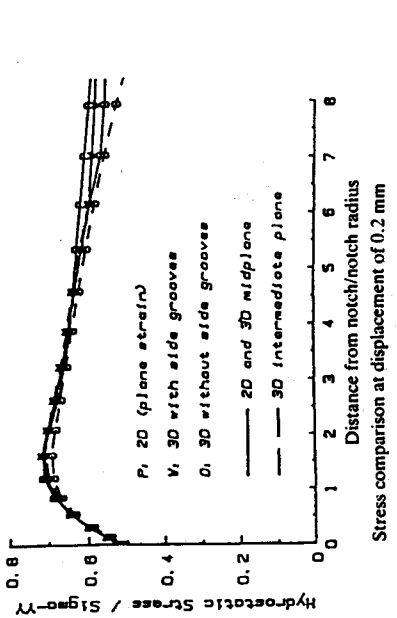

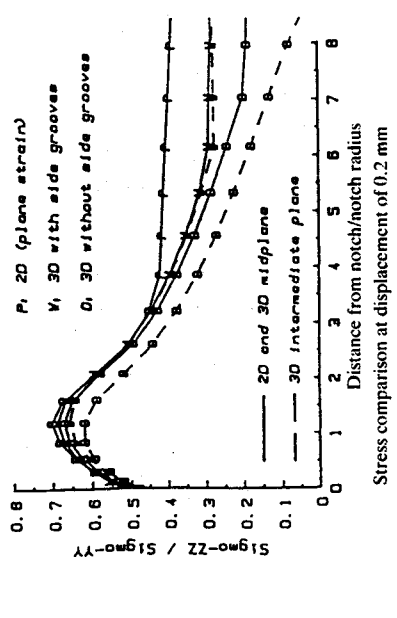

Fig 2 2D and 3D model notch region stress behaviour at an applied displacement level of 0.2 mm (general yield load conditions)

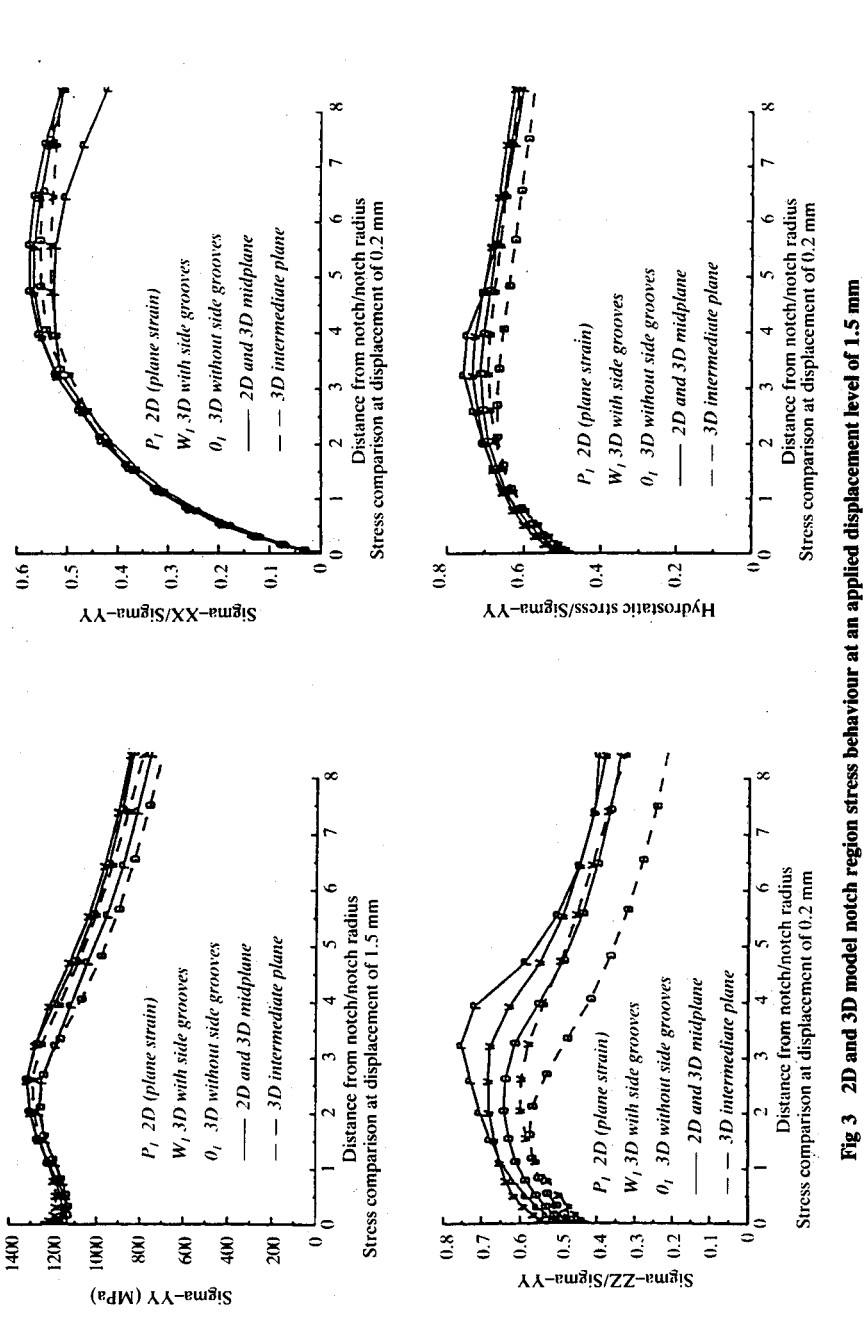

Fig 3 2D and 3D model notch region stress behaviour at an applied displacement level of 1.5 mm

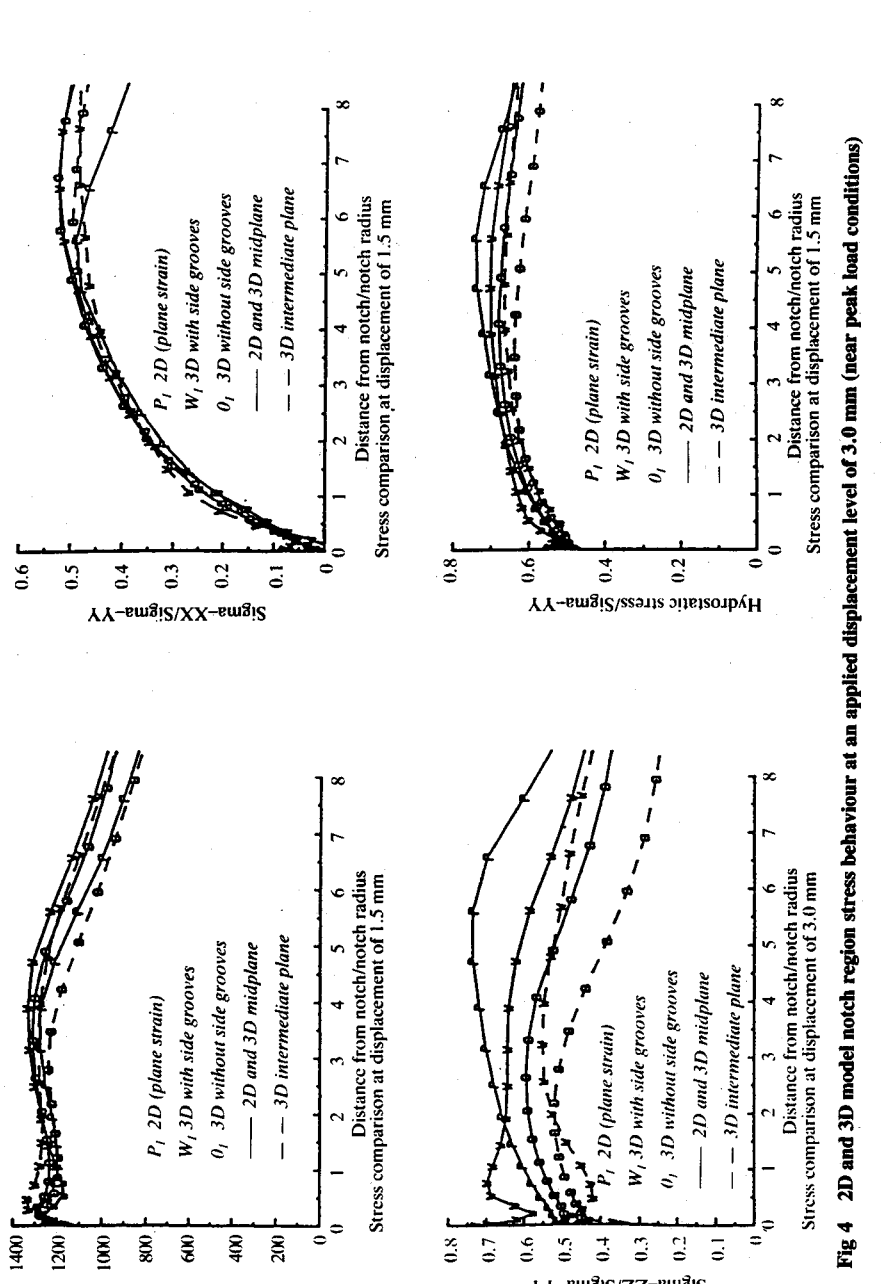

Fig 4 2D and 3D model notch region stress behaviour at an applied displacement level of 3.0 mm (near peak load conditions)

position along the notch front, stresses from the 3D midplane (solid line) are plotted, as well as stresses from a position about half way between the midplane and the surface plane (dashed line). All three normal stress components are plotted in addition to the hydrostatic stress. The hydrostatic stress is the average of the three normal stresses and is considered to be an effective measure of constraint.

Figure 2 compares the 2D and 3D fracture plane stress distributions for a full size standard specimen at about the general yield load. The stress distributions are plotted versus the distance from the notch tip, where the notch tip is normalized by the original notch tip radius (0.25 mm). The portion of the stress distribution important to fracture behaviour is that between the notch tip and the peak stress (σ_{yy}) location. For this load level, the peak stress location is about 1.5 notch root radii from the notch surface. At least the centre half thickness of both 3D geometries (with side grooves and without) is very near to plane strain conditions. At this load level, even the through thickness stress (σ_{zz}) is very close to that of the 2D plane strain solution. The side grooves provide a slight improvement of the σ_{zz} distribution at the intermediate plane.

Figure 3 compares the 2D and 3D fracture plane stress distributions at a displacement of 1.5 mm which is about 8 times the displacement at general yield. At this load level, the peak σ_{yy} stresses occur at about 2.5 times the initial notch root radii from the notch surface. Except for the effect on the through thickness stress (σ_{zz}), the increased plasticity associated with this load level has led to very little loss of plane strain behaviour compared to that at general yield. To the extent that the hydrostatic stress behaviour is believed to be a more important measure of plane strain behaviour than the through thickness stress, it can be reasonably argued that the centre half of the 3D specimen notch fronts are still predominately plane strain. At this load level, the side grooves are again seen to provide an improvement of the σ_{zz} distributions.

Figure 4 compares the 2D and 3D fracture plane stress distributions at a displacement of 3.0 mm which is about 15 times the displacement at general yield. At this load level, the peak σ_{yy} stresses occur at about 3.5 times the initial notch root radii from the notch surface. The 'bump' in the σ_{yy} stress distributions near the notch surface is believed to be the result of excessive distortion in the finite elements near the notch tip. To the extent that the element distortion affects the 2D and 3D solutions similarly, it is believed that this numerical anomaly does not affect the conclusions to be drawn from these solutions. Again, except for the effect on the through thickness stress (σ_{zz}), the increased plasticity associated with this load level has led to very little loss of plane strain behaviour at the examined sections. The improvement in the σ_{zz} stress distribution for the side grooved specimen at high loads is apparent in Fig. 4. The 3D side groove solution behaviour at small distances from the notch seen for the σ_{zz} stress is believed to be the result of the relatively coarse side groove modelling contributing to the above noted element distortion effects.

In summary, it can be concluded from the finite element solutions that the

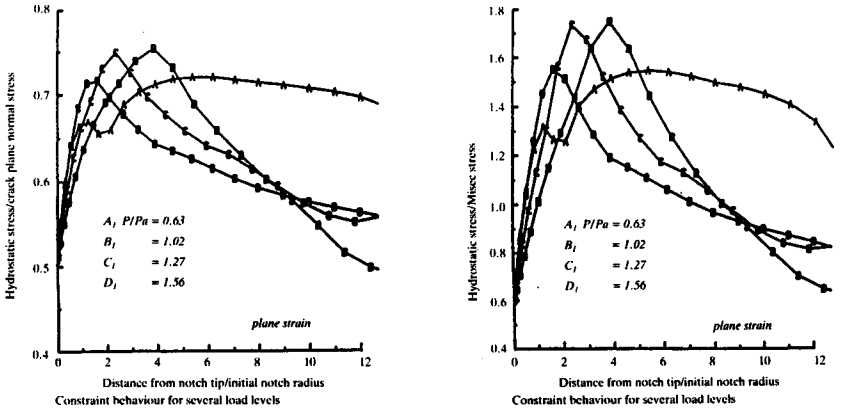

Fig 5 Notch tip region behaviour of hydrostatic stress at four load levels (refined 2D plane strain model of the standard Charpy specimen)

centre-half portions of the notch fronts for side grooved and non-side grooved specimens exhibit plane strain behaviour for applied displacement levels up to those representative of general yield. Beyond general yield load, the through thickness stresses are much closer to plane strain when the specimen is side grooved. Further comparisons using stress contours on the fracture plane will be made below. The beneficial effect of the side grooves will become more apparent during that discussion.

Central notch region stress behaviour

The relevance of the 2D plane strain idealization to the central notch front region stress states has been demonstrated. In this section stress behaviour from a refined 2D plane strain model are presented. This refined model was used to examine the effect of load level on notch tip region constraint. Four load levels were considered. The lowest load level was 0.63 of the Green and Hundy (G&H) (**9**) general yield load (P_0) and therefore showed very limited plasticity effects. The highest load level was for a load ratio of 1.56. This highest load level corresponds to an applied displacement of 3 mm. Figure 5 shows the crack plane hydrostatic stress behaviour as a function of the distance from the notch tip. As noted previously, the hydrostatic stress is an indicator of constraint. Normalizing the hydrostatic stress with the crack plane normal stress (σ_{yy} makes the shift of the region of peak constraint more clear. Since the Mises stress is a measure of the tendency for the material to strain plastically, and since the hydrostatic stress does not affect plastic behaviour, normalizing the hydrostatic stress by the Mises stress allows the constraint related stress magnitudes to be compared to the plasticity related stress magnitudes. It can be seen that the constraint related stresses are 1.6 and 1.8 times the magnitude of the plasticity related stresses after general yield is reached. It can be seen that

plasticity initially increases constraint near the notch tip while lowering it at locations farther from the notch tip. Then further plasticity causes the location of the highest constraint to move farther from the notch tip.

Benefits associated with side grooving

Putting side grooves in the MNT* specimens has two fundamental effects. By reducing the fracture plane area, the load required to achieve a critical stress state is reduced. At the same time, the cross-section at the region where plastic collapse can occur in the non-side grooved specimens is not reduced. Therefore, shear stress in the plastic zone to either side of the fracture plane is significantly reduced by the addition of side grooves. This results in an increase in the plastic collapse load relative to the fracture load. The second fundamental effect, as will be demonstrated in the following discussion, is that a larger portion of the notch front has plane strain fields.

In the following, crack plane stress fields from the 3D models of a standard Charpy specimen and a standard specimen with 20 percent side-grooves are compared. The purpose of the comparison is to show how the introduction of side grooves affects the variation in stress field behaviour in going from the specimen midplane to the external specimen surface. Since the crack plane normal stress (σ_{yy}) and the hydrostatic stress are considered to be the most important stress quantities for illustrating plane strain behaviour, only these stresses are compared.

Figures 6 through 9 compare the crack plane σ_{yy} and hydrostatic pressure contours for the refined 3D model with side grooves and the refined 3D model without side grooves. Figures 6 and 7 show the behaviour at the displacement of 0.2 mm (approximately at general yield), and Figs 8 and 9 show the behaviour at 1.5 mm of displacement. The plots at the bottom of these figures are the results without side grooves and those at the top are with 20 percent side grooves. The notch front is the right edge of each contour plot while the left edge is at the tup contact region. The bottom edge of these plots corresponds to the specimen midplane. For the model without side grooves, the top edge of the plot is the external surface of the specimen. For the model with side grooves, the top edge of the plot corresponds to the root of the side groove.

In Figures 6 and 7 it can be seen that there is a significant reduction in the σ_{yy} and hydrostatic stress between the quarter thickness plane (intermediate plane of Figs 2, 3 and 4) and the external surface of the specimen. For the side grooved specimen, the stress near the notch show little variation between the midplane and the side groove root. Since Fig. 2 shows that both 3D models have plane strain behaviour at the midplane, it can be concluded that adding side grooves resulted in an increase in the portion of the notch exhibiting plane strain behaviour. In Figs 8 and 9, it can be seen that the loss of plane strain

* The techniques described here are protected by US patent numbers 4,864,867 and 5,165,287.

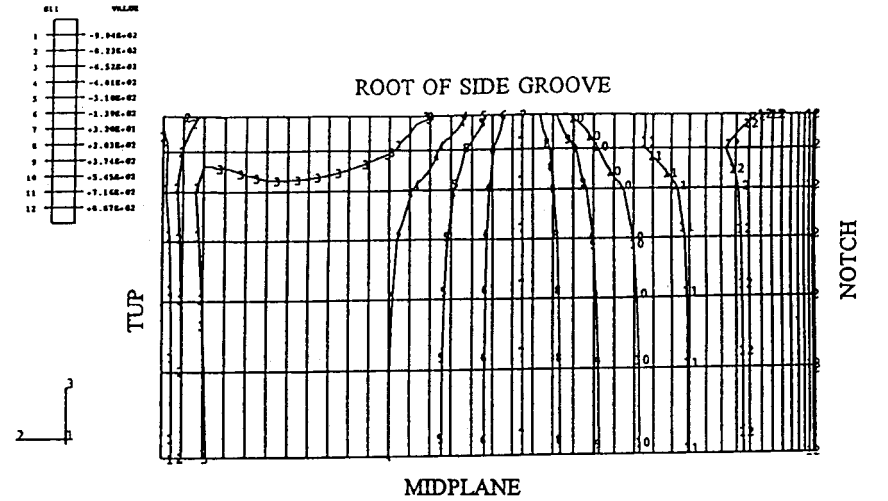

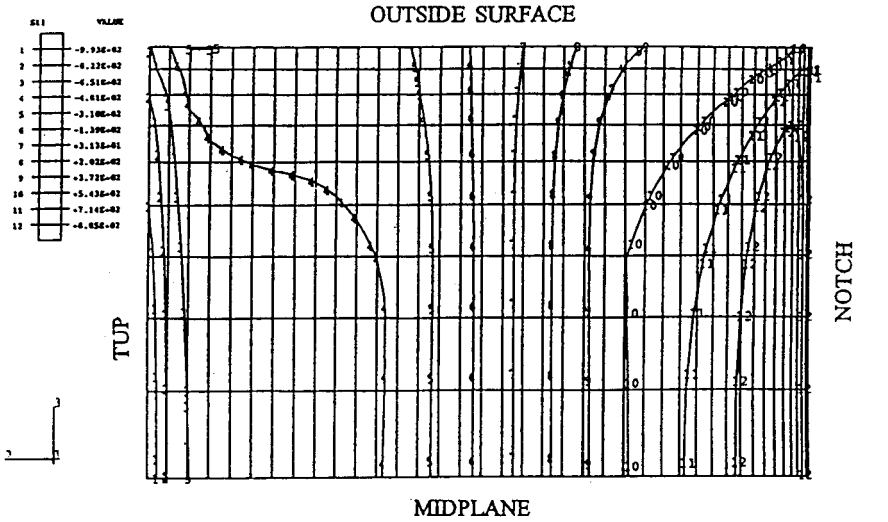

Fig 6 Comparison of fracture plane σ_{yy} contours at a displacement of 0.2 mm for notched specimens both with (top) and without (bottom) side grooves

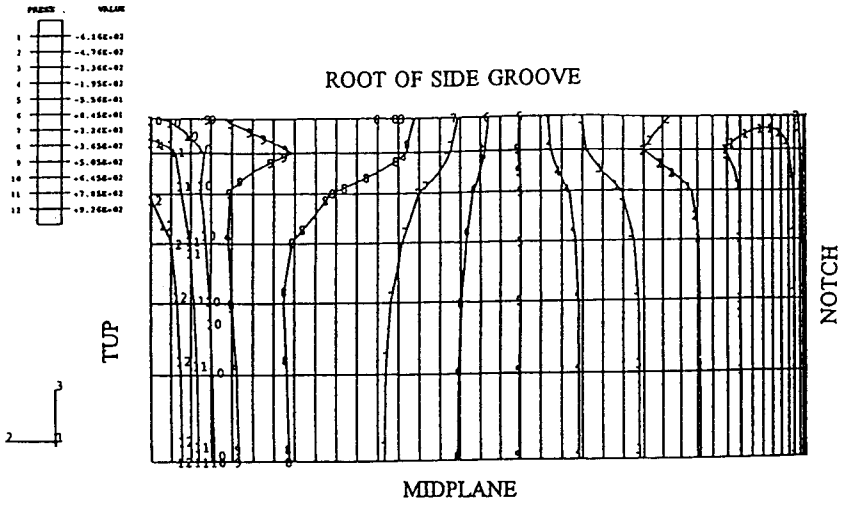

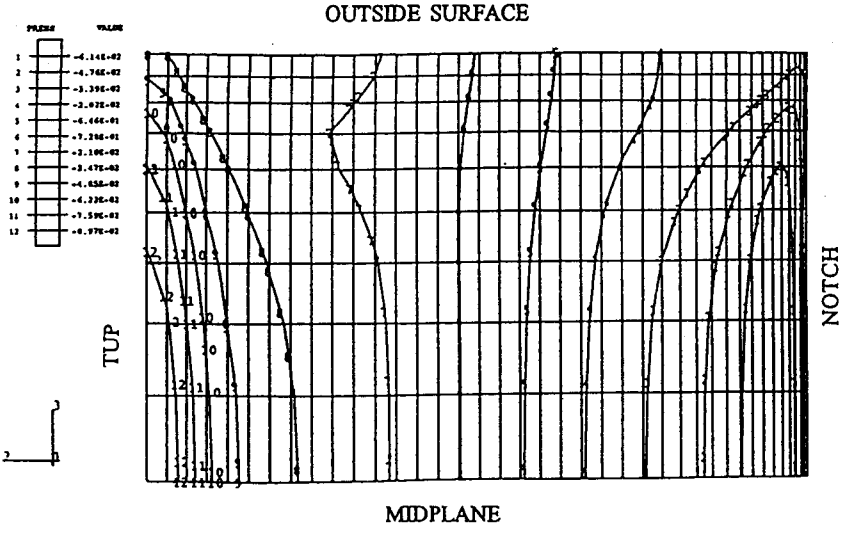

Fig 7 Comparison of fracture plane hydrostatic pressure contours at a displacement of 0.2 mm for notched specimens both with (top) and without (bottom) side grooves

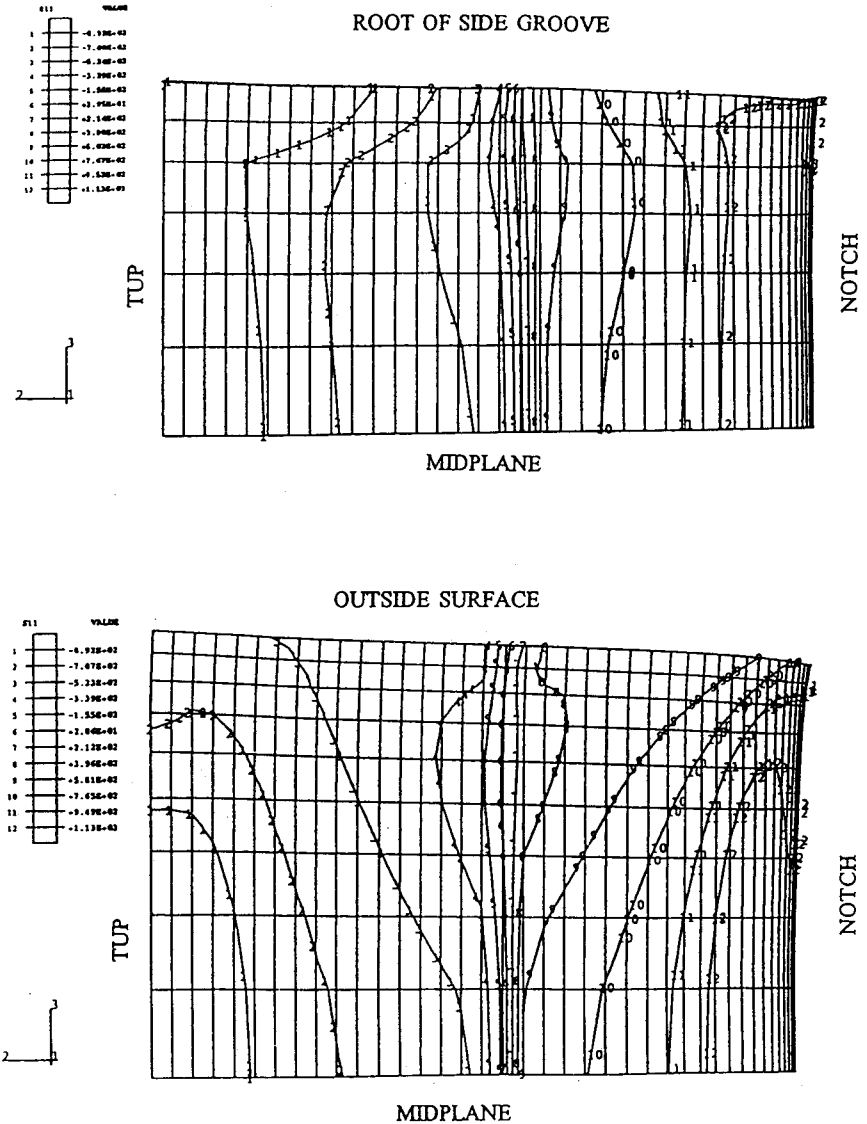

Fig 8 Comparison of fracture plane σ_{yy} contours at a displacement of 1.5 mm for notched specimens both with (top) and without (bottom) side grooves

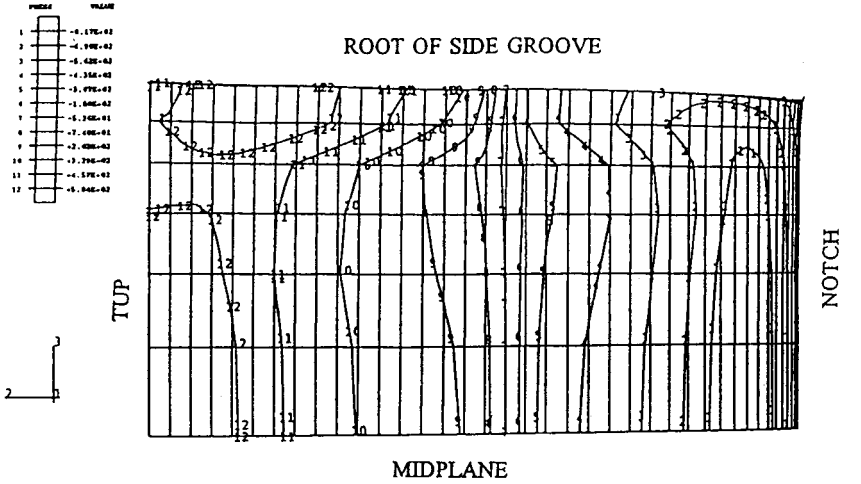

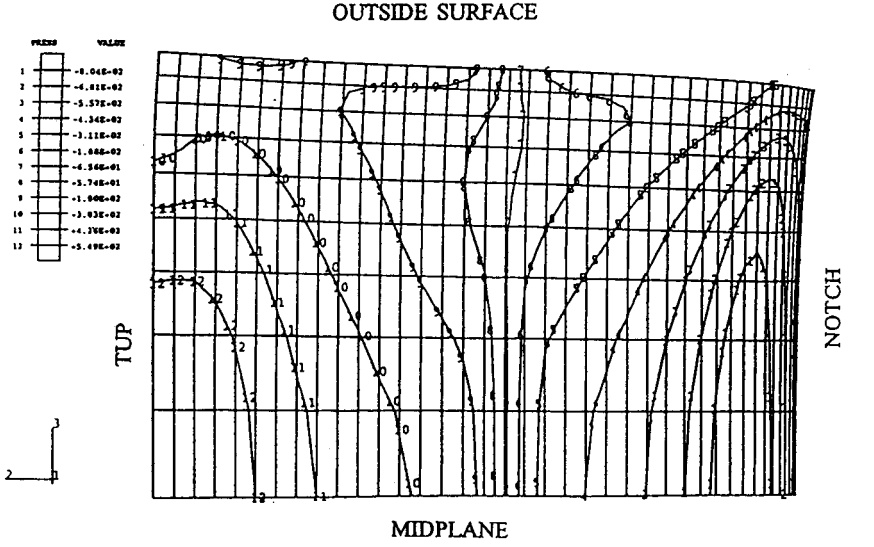

Fig 9 Comparison of fracture plane hydrostatic pressure contours at a displacement of 1.5 mm for notched specimens both with (top) and without (bottom) side grooves

behaviour over the outer quarter thickness of the model without side grooves is greater than it was for the smaller displacement level. Although there is some reduction in the hydrostatic stress for the side grooved specimen near the side groove, the loss is much less significant than for the model without side grooves. Calculations at 3 mm of displacement showed that the loss in plane strain behaviour in the outer quarter thickness of the side grooved and non-side grooved models is not substantially different from that at the displacement level of 1.5 mm. This strongly suggests that further displacement increases would not result in substantially different plane strain behaviour than observed at 1.5 and 3 mm of displacement.

The observation that the loss of plane strain behaviour does not appear to continue after a displacement of about 8 times the general yield displacement is important. This is because dimensional analysis shows that miniature specimens will require relatively larger displacements than full scale specimens to achieve comparable crack tip field intensities. Further, the use of side grooves results in a larger volume of material being sampled at near plane strain conditions. We estimate that for the miniature specimen with side grooves the peak hydrostatic stress field extends along the notch to 80 percent of the distance calculated in the conventional specimen. Whereas the peak hydrostatic stress field in the miniature specimen without side grooves extends along the notch to half the distance of the conventional specimen. This relative increase in the peak stress region size due to size grooves is expected to reduce scatter (and therefore less specimens will be needed) for specimens tested in the transition region where the trigger particle mechanism dominates brittle fracture initiation.

Striker design and contact conditions

In our recent finite element study, which was focused on non-linear response prior to crack initiation, two sensitivity studies related to tup design were performed. The first study compared the load versus deflection behaviour from the ISO and ASTM tup designs. For loading up to displacements representative of peak Charpy test loads, the ISO tup was found to result in load levels that were about 5 percent below those of the ASTM tup. This load decrease was attributed to the fact that the relatively flat contact region of the ASTM tup is about 10 percent of the support span width. This flat contact region results in the contact forces being significantly concentrated near the ends of the contact region. This concentration, in effect, results in a four point bending condition. If the contact forces were exactly concentrated at the corners, the applied moment for a given load level would be 10 percent less than for the three point bending condition. The smaller 5 percent effect that was observed in the finite element simulation is easily accounted for by the fact that contact forces, while peaked at the corners, do exist all along the contact region.

In the second finite element sensitivity study, the ASTM tup design was used

with two levels of friction. In one case, the friction coefficient was zero while in the other, the coefficient was 0.5. In the latter case, the maximum friction force was further limited by the shear yield strength of the specimen material. Since the frictional forces were observed to be largely limited by this yield stress value, the assumed coefficient had little effect on the results. The calculations showed that the addition of frictional forces increased the applied load levels by about 10 percent. This load increase was attributed to frictional forces at the support points restraining the longitudinal expansion of the notched side of the specimen.

Both of these results are consistent with several experimental observations that have appeared in the literature for which the Charpy energies for the two tup geometries have been compared. Tower (**10**) showed that different Charpy energies can result from using the ISO and the ASTM tups when testing highly ductile materials. While for energy levels below 60 J, differences were negligible, for energies in the 100 to 200 J range, energies were as much as 25 percent larger for the ASTM tup. The explanation given for this increase in energy was the intense localized deformation caused by the corners of the ASTM tup design. These corners allowed the tup to essentially gouge the contact surface as the result of the contacted surface of the specimen wanting to contact under the bending induced compression at this surface. This gouging action results in significant plastic deformation and energy dissipation. While the higher Charpy energy levels of the Tower study were for materials other than vessel steels, similar behaviour with energy differences in the 10 to 15 percent range have been observed for nuclear pressure vessel steels on the upper shelf (**11**).

By restricting the contraction of the specimen's contacted surface, the ASTM tup results in a net tensile stress being superimposed on the fracture plane bending stress distribution. This additional tension might be expected to decrease the chance that a specimen will wrap around the tup rather than break into two pieces. This behaviour has been observed by researchers at the Belgian Nuclear Research Centre (**12**). It is not clear how this superimposed tensile stress would be reflected in the Charpy energy differences since the higher loads of the ASTM design would be truncated at the time of separation while the lower load levels of the ISO design would continue until the specimen slips off the supports.

Some direct evidence exists for the contact surface gouging being the primary cause of the higher energies for the ASTM tup design. In their specimen reconstitution work, Belgian Nuclear Research Centre researchers have found that localized hardening due to welding near the tup contact region can reduce the degree of gouging (**13**). When the gouging is avoided, the ISO and ASTM tups result in essentially the same Charpy energies. To further confirm this conclusion that the gouging and higher energies are linked, tests were done in which a hard tungsten foil was placed between the ASTM tup and the specimen. Again the gouging was avoided, and the Charpy energies were essentially the same as those from using the ISO tup design.

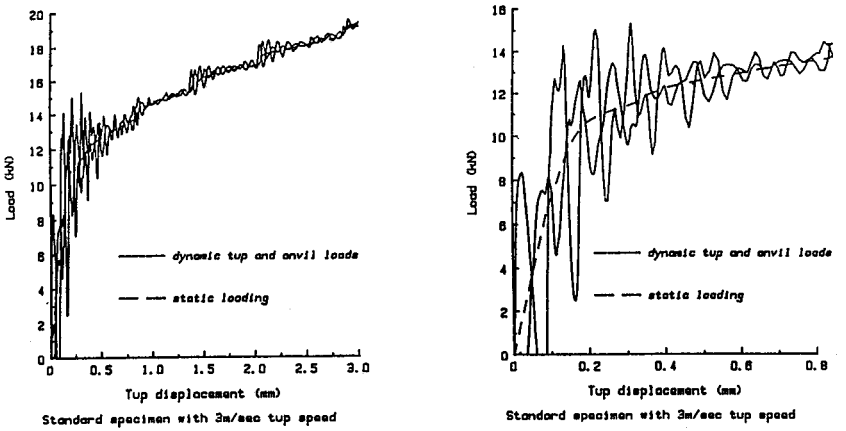

Fig 10 Dynamic load versus tup displacement behaviour for the standard specimen being struck with a tup speed of 3 m/sec

With the above observations, it was decided that our miniature specimen testing program would focus on using the ISO and ASTM tup design. One reason for this choice is that the energy that one obtains from a Charpy test is intended to be indicative of the fracture resistance of the material. The fact that a part of the energy obtained from some tests using the ASTM tup design is totally unrelated to the fracture process is seen as an unattractive feature. Perhaps the more compelling reason is that miniature specimens will tend to behave in a more ductile manner than full scale specimens, therefore tending to exaggerate this undesirable gouging behaviour in the miniature specimens. If there is a negative side to using the ISO tup in the miniature specimen testing, it is probably that there may be a greater chance that the specimen will not fracture to the point of becoming two pieces. This behaviour would be expected to be more likely for the miniature specimens than full size specimens due to the relatively more ductile behaviour of the smaller specimen.

Inertial effects

Figures 10 and 11 show the results of two dynamic analyses. Both analyses assume plane strain conditions. Quasi-static stress-strain properties were used for these simulations. The data presented in Fig. 10 is for a constant tup velocity of 3 m/sec which is the low end of the tup velocity range stipulated by the ASTM standard E23. Figure 11 resulted from assuming a constant tup velocity of 6 m/s, the upper end of the stipulated velocity range. The load-deflection curves from the static analyses are included in these plots for comparison with the dynamic curves. For the static loading case, the tup and anvil loads are equal (but in opposite directions). This is not generally the case for the dynamic analysis due to the inertial effects and therefore both loads are

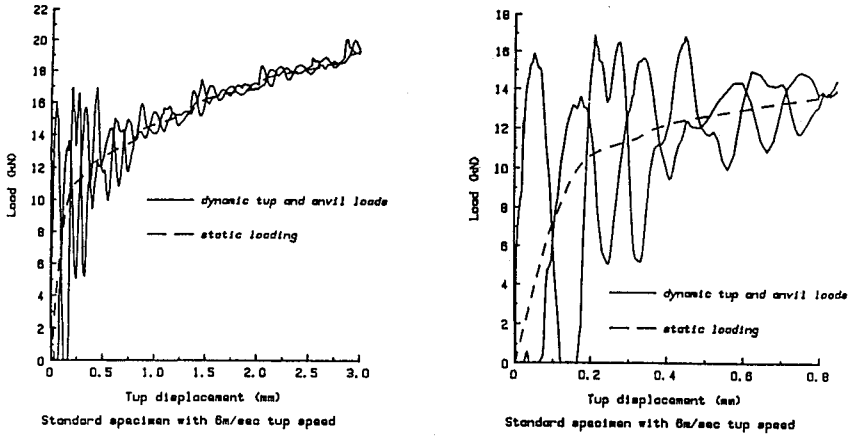

Fig 11 Dynamic load versus tup displacement behaviour for the standard specimen being struck with a tup speed of 6 m/sec

plotted. It can be seen that the tup and anvil loads tend to be out of phase with respect to each other. For earlier times (small deflections), the oscillation of the loads is very large. However, once plastic deformation becomes significant, the high frequency oscillations are quickly damped out. Another factor which contributes to the dynamic behaviour approaching quasi-static loading behaviour is that the loading rate is relatively slow compared to the stress wave speeds. Elastic stress wave speeds are between 3×10^6 mm/sec and 6×10^6 mm/sec depending on the type of wave (compressive, shear, or surface). At this speed, stress waves can propagate to the end of the specimen and return to the notch region 25 to 55 times by the time the tup displaces the specimen 3 mm.

Examining the right side plots of Figs 10 and 11, it can be seen that the anvil does not exert a reaction until a tup displacement of about 0.04 or 0.08 mm. This reflects the time that it takes for the stress wave from initial contact to propagate to the anvil contact location. These plots also show that the first oscillation in the tup load results in the tup load going to zero for a period of time. This is the result of the specimen springing away from the tup shortly after initial contact. This springing away is the result of the first stress wave returning to the tup contact region after having reflected from the end of the specimen.

It is worth noting that the size of the tup load oscillations found in these dynamic simulations are larger than typically measured during instrumented Charpy testing. The fact that the size of the oscillations obtained experimentally seem to depend to some extent on the group doing the work suggests that perhaps 'electrical damping' in the measurement systems may be a partial explanation. In fact, many researchers have used signal conditioners which operate in the few tens of kHz range. Our calculations show that the load transducer signal is in the 20 to 40 kHz range. Therefore, a system capable of at

least 100 kHz, with a 1 MHZ sampling rate, is needed to accurately determine the general yield load.

To verify scalability of the full size dynamic Charpy solution to a half size specimen, a half scale version of the coarse 2D grid was generated. All dimensions, including those of the tup and anvil, were halved. For static loading, the stress and strain solution scaled exactly with that of the full scale model. The dynamic simulation, run with a tup velocity of 6 m/sec, verified that the dynamic solution also scales exactly if both specimen sizes are impacted with tups having the same velocity. The principal conclusion to be drawn from this analysis is that the tendency for inertial effects to become negligible after general yield also occurs for the half scale specimen.

Summary and conclusions

Design of all miniature specimens should begin with a thorough examination of the material microstructure to determine the minimum specimen dimension. In the case of the MNT, the proposed minimum cross-section dimension is 5 mm × 5 mm for RPV materials to ensure that chemical bands and inclusion stringers within the steel are adequately represented. In order to simulate the stress state of the conventional specimen, a 1/2 scale factor has been proposed. The 1/2 scale factor applies to the specimen dimensions as well as to the span and tup radius. In addition to scaling the key test parameters, 20 percent side grooving is recommended to substantially increase the volume of material which is exposed to plane strain conditions. Miniature specimens tested on the upper shelf which are side grooved will produce an absolute length of plane strain along the notch which is about 80 percent of that experienced in conventional 10 mm × 10 mm × 55 mm specimens. Therefore, side grooves will significantly offset the reduction in plane strain at the notch/crack tip for miniature specimens.

Generally, it is expected that a smaller specimen will tend to behave as though the material is tougher. This is the fundamental result of the nonscalability of the material microstructure and the mathematics associated with singular crack tip fields. In terms of transition temperature behaviour, this means that the transition temperature measured with a smaller specimen will tend to be lower than the transition temperature measured with a larger specimen. The design of the miniature specimen has focused on minimizing this shift. The most significant design aspects in terms of reducing this shift are the side grooves, and the use of proportional scaling. Basically, the side grooves will make the smaller specimens behave as though the material is less tough, as compared to the behaviour that would be obtained if a perfectly scaled Charpy geometry were used.

Although the feasibility of preparing 16 miniature specimens from the broken halves of one conventional specimen has been experimentally demonstrated, detailed analysis of the miniature specimen stress fields has shown that

the conventional specimen aspect ratio results in a favourable bending-to-shear ratio. The larger aspect ratio limits the number of specimens which can be machined from a conventional specimen to 8 (4 from each broken half). However, the larger miniature specimens have the significant advantage that they can be weld reconstituted since the requirement of providing an insert of 2 times the width (W) can be satisfied. Therefore, it is now possible to produce 24 miniature specimens (as opposed to 16 earlier) from one conventional specimen using the weld reconstitution procedure. This strategy is particularly effective in nuclear reactor pressure vessel surveillance in cases where a limited fixed volume of material is available. A surveillance capsule can be withdrawn, the specimens tested, and 8 miniature specimens (4 from each half) can then be machined from the broken halves of each specimen. Then, after further irradiation, the specimens can be tested and weld reconstituted (16 reconstituted specimens from the original 8 miniature specimens) to produce an additional 24 specimens for re-irradiation and testing. Thus, using this strategy, it will be possible to produce sufficient data for accurate trend curve development on a plant-specific basis.

Acknowledgments

The authors are grateful to the Empire State Electric Energy Research Corporation (ESEERCO) and the New York state utilities for their sponsorship of this work. We are also grateful to Dr. L.J. Cuddy (Metallurgical Consultants) for his technical assistance with the microstructural work. We also wish to thank Mr. A.J. Peterson for his recognition of the importance of this work and his efforts in championing the technology.

References

(1) LUCAS, G. E., ODETTE, G. R., SHECKHERD, J. W., McCONNELL, P., and PERRIN, J. (1986) Subsized Bend and Charpy V-Notch Specimens for Irradiated Testing, *The Use of Small-Scale Specimens for Testing Irradiated Material*, ASTM STP 888, (Edited by W. R. Corwin and G. E. Lucas), American Society for Testing and Materials, Philadelphia, 305–324.

(2) CORWIN, W. R. and HOUGLAND, A. M. (1986) Effect of Specimen Size and Material condition on the Charpy Impact Properties of 9Cr-1Mo-V-Nb Steel, *The Use of Small-Scale Specimens for Testing Irradiated Material*, ASTM STP 888, (Edited by W. R. Corwin and G. E. Lucas), American Society for Testing and Materials, Philadelphia, 325–338.

(3) HARLING, O. K., LEE, M., SOHN, D-S., KOHSE, G., and LAU, C. W. (1986) The MIT Miniaturized Disk Bend Test, *The Use of Small-Scale Specimens for Testing Irradiated Material*, ASTM STP 888, (Edited by W. R. Corwin and G. E. Lucas), American Society for Testing and Materials, Philadelphia, 50–65.

(4) MANAHAN, M. P. and CHARLES, C. (1990) A Generalized Methodology for Obtaining Quantitative Charpy Data From Test Specimens of Nonstandard Dimensions, *Nuclear Technology*, **90**, May.

(5) (1993) *Small Specimen Test Techniques Applied to Nuclear Reactor Vessel Thermal Annealing and Plant Life Extension*, American Society for Testing and Materials, ASTM STP 1204.

(6) FLEMINGS, M. C. (1979) *Solidification Processing*, McGraw-Hill, 149.

(7) MANAHAN, M. P. (1989) Determination of Fracture Behaviour of Ferritic Steels Using Miniaturized Specimens, *Journal of Nuclear Materials* **166** 321–330.

(8) MANAHAN, M. P., WILLIAMS, J., and MARTUKANITZ, R. P. (1993) Laser Weld Reconstitution of Conventional Charpy and Miniaturized Notch Test (MNT) Specimens, *Small Specimen Test Techniques Applied to Nuclear Reactor Vessel Thermal Annealing and Plant Life Extension*, ASTM STP 1204, (Edited by W. R. Corwin, F. M. Haggag, and W. L Server), American Society for Testing and Materials, Philadelphia, 62–76.

(9) GREEN, A. P. and HUNDY, B.B. (1956) Initial Plastic Yielding in Notched Bend Tests, *Journal of the Mechanics and Physics of Solids*, **4**, 2, March 128–144.

(10) TOWERS, O. L. (1983) Effects of Striker Geometry on Charpy Results, *Metal Construction*, **15**(11).

(11) VAN WALLE, E., FABRY, A., VAN DE VELDE, J., CHAOUADI, R., PUZZOLANTE, J. L., and VAN RANSBEECK, T. (1993) Pressure Vessel Steel Programme at the Belgian Nuclear Research Centre, March 8.

(12) MANAHAN, M. P., MPM Research & Consulting, and VAN WALLE, E. SCK/CEN (1994). Private Communication.

(13) VAN WALLE, E., FABRY, A., VAN RANSBEECK, T., PUZZOLANTE, J-L., VANDERMEULEN, W., and VAN DE VELDE, J. (1991) The Reconstitution of Small Remnant Parts of Charpy-V Specimens, presented at SMIRT 11, PCS II, Taipei, Taiwan, August.